Study of Corrosion Resistance of Lean Duplex Stainless Steel 2101 Welded by the Gas Tungsten Arc Welding Double Fusion (GTAW-DF) Process for Use in the Citrus Juice Industry

A. F. S. Bugarin[a,b]* [iD] *, B. V. G. Viveiros[a]* [iD] *, M. Terada[b]* [iD] *, G. L. X. Ribeiro[b]* [iD] *,*

L. H. Guilherme[c] [iD] *, M. D. M. Neves[a]* [iD] *, I. Costa[a]* [iD]

[a]Instituto de Pesquisas Energéticas e Nucleares (IPEN-CNEN), 05508-000, São Paulo, SP, Brasil.
[b]Instituto SENAI de Inovação em Manufatura Avançada e Microfabricação, 04757-000, São Paulo, SP, Brasil.
[c]ACW Engenharia, 14802-580, Araraquara, SP, Brasil.

This work aims to investigate the influence of optimized welding parameters on the corrosion performance of the lean duplex stainless steel (LDSS) UNS S32101. The correlation between microstructure and electrochemical behavior of the fusion line (FL) and fusion zone (FZ) has been investigated. In the study, six welded samples were manufactured with different welding parameters, specifically the welding current, travel speed and heat input. A mini-cell and Syringe Cell were used to characterize the electrochemical behavior of the different welded zones by means of the double loop electrochemical potentiokinetic reactivation test (DL-EPR) and potentiodynamic polarization tests. The results showed that the welding parameters tested in this study significantly affected the corrosion resistance of the LDSS UNS S32101. The heat-affected zone (HAZ) was the most susceptible zone to localized corrosion and the specific region most affected by corrosion process was that of the LDSS UNS S32101 adjacent to the FL.

Keywords: *Lean duplex stainless steel, LDSS UNS S32101, GTAW-DF, corrosion resistance.*

1. Introduction

Tanks for storing products in the food industry are usually made of stainless steel, as they must have hygiene and safety standards to ensure product quality. These stainless steels have been increasing demand due to their good combination of mechanical properties, weldability and corrosion resistance. Many tanks in operation are constructed with austenitic stainless steels. However, there is a tendency to replace it with duplex stainless steels (AID), due to its superior mechanical properties and high corrosion resistance[1-4].

The AIDs have great technological importance due to their balanced combination of dual-phase microstructure[3,5]. The two primary phases in duplex stainless steel are austenitic and ferritic, resulting in a balanced combination of high strength and corrosion resistance, that combines features of both austenitic and ferritic stainless steels. The main alloying elements in duplex steels are chromium, nickel, molybdenum, and nitrogen[5,6]. When it comes to welding, duplex stainless steels present some unique considerations compared to other types of stainless steels, such as austenitic and ferritic grades. Austenitic stainless steels are less prone to cracking during welding. However, excessive heat input can lead to sensitization and intergranular corrosion in the heat-affected zone. On the other hand, ferritic stainless steels are also generally considered weldable. However, they are more susceptible to grain growth and sensitization during welding compared to austenitic grades[6,7].

Duplex stainless steel is a type of stainless steel that combines features of both austenitic and ferritic stainless steels. The main alloying elements in duplex steels are chromium, nickel, molybdenum, and nitrogen. The two primary phases in duplex stainless steel are austenitic and ferritic, resulting in a balanced combination of high strength and corrosion resistance. When it comes to welding, duplex stainless steels present some unique considerations compared to other types of stainless steels, such as austenitic and ferritic grades[6,7].

The welding in the AID significantly modifies original microstructure in the welded joint and adjacent regions due to the various thermal cycles to which the metal is subjected during process[8]. These changes of the microstructure can decrease the corrosion resistance in the welding zones. In the case of AIDs, depending on the parameters used, the precipitation of deleterious phases may occur, reducing the steel properties, including its corrosion resistance[2,9]. Some studies suggested that the heat-affected zone (HAZ) is the region most susceptible to localized corrosion in welded joints[10-14]. Therefore, the choice of parameters is important and must be careful to guarantee the excellent properties of the duplex stainless steel. There are studies that correlate decomposition and the formation of phases in the corrosion resistance of the UNS S32101, UNS S32205 and UNS S32520 stainless steels, after heat treatment[15-17].

The literature about welding effects of heat input on microstructure, mechanical properties[18-20], and corrosion in stainless steel; Mohammed et al.[21] presented that low heat

*e-mail: afbugarin@usp.br

input in the welding should be avoided, since it would cause a rapid cooling rate and therefore would not have sufficient austenite in the weld filler metal, the heat affected zone (HAZ), and would lose the balance of austenite and ferrite, which is characteristic of AID. In studies about friction stir welded AIDs[22], it was observed that the corrosion resistance of welded joints was better than base material and it increased with increasing in the heat input.

The Gas Tungsten Arc Welding double fusion method (GTAW-DF) have been investigated to weld AIDs. In GTAW-DF, two heat sources are employed, which are positioned on opposite sides, allowing operators to perform the root pass and the welding simultaneously. The advantages of this process are a better-quality finishing, greater depth of penetration, greater welding efficiency and less microstructure distortion[23,24]. Guilherme et al.[1] investigated corrosion performance of UNS S32101 duplex welded by GTWA-DF and verified that the joint with higher heat input and low current demonstrated better corrosion performance when compared to the joint with lower heat input and higher current. This work aims to investigate the influence of GTAW-DF welding parameters on LDSS duplex steel UNS S32101 used in the construction of tanks for the citrus juice industry from the point of view of corrosion resistance.

2. Materials and Methods

The materials used in this work were lean duplex stainless-steel grade UNS S32101 (LDSS UNS S32101) and weld filler metal ER2209, whose composition are shown in Table 1. Six (6) specimens (CP) were produced with parameters shown in Table 2. The GTAW welding procedure was double-fusion method (DF). The welding process was performed simultaneously by two welders: on the chamfer side, the main arc welder, responsible for depositing the filler material and initiating the process; on the root side, the auxiliary arc welder, who moves synchronously with the main arc welder, but with a delay that results in a distance of 5 to 25 mm from the main arc. In Figure 1 is showing the schematic illustration of the welded parts, indicating the chamfer angle of 35°, the root distance of 1 mm and the distance between the MB of 3.2 mm. Three specimens were welded with two passes, Figure 1b (CP 01, CP 02 and CP 03), and another three specimens were welded with only one pass, Figure 1c (CP 04, CP 05 and CP 06), and Figure 1d is presented schematic representation of the GTAW-DF. Welding parameters (current intensity, arc voltage and welding speed) were selected based on the adequate evolution in carrying out welding, aiming at reducing discontinuities and increasing manufacturing productivity.

Table 1. Nominal chemical compositions (wt%) of LDSS UNS S32101 and filler metal ER2209.

	C	Cr	Ni	Mo	Mn	P	S	Si	N	Cu
S32101	0.019	21.32	1.15	0.19	4.87	0.024	0.001	0.73	0.22	0.53
ER2209	0.020	22.90	8.60	3.20	1.60	0.017	0.001	0.40	0.16	0.10

Table 2. GTAW root pass welding parameters.

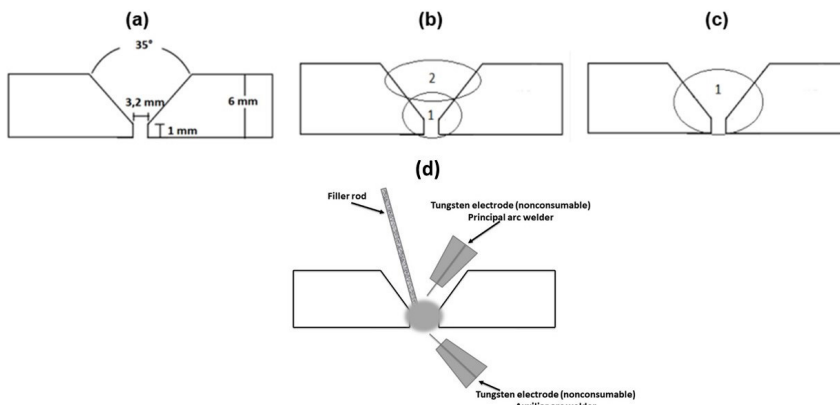| CP	Welding pass (number)	Current (A)		Voltage (V)		Travel speed (cm/min)	Heat input KJ/mm
01	01	140	130	18	12	8.82	1.4
	02	140	140	11	11	3.03	3.0
02	01	230	220	18	18	19.04	1.3
	02	230	230	16	16	9.52	2.6
03	01	320	300	22	19	17.1	2.2
	02	320	320	20	20	9.3	4.1
04	01	230		17		15.2	1.5
05	01	230		15		23.0	0.9
06	01	230		17		31.5	0.7

Figure 1. (a) schematic illustration of the welded parts. Pass sequence to (b) two passes (CP 01, CP 02 and CP 03) and (c) one pass (CP 04, CP 05 and CP 06), and (d) schematic representation of the GTAW-DF.

Study of Corrosion Resistance of Lean Duplex Stainless Steel 2101 Welded by the Gas Tungsten Arc Welding
Double Fusion (GTAW-DF) Process for Use in the Citrus Juice Industry

3

The preparation of all CPs was carried in the cross section of the welding joint. The specimens were grinded up to #4000 to perform electrochemical tests and polished up to 0.25 μm to metallographic characterization. Metallographic etching was performed in a 10 wt% oxalic acid solution, by applying a current density of 1.0 A/cm^2 for 20 s, at room temperature. These results were observed with optical microscope (OM) *Leica* DMLM model.

Vickers microhardness measurements were performed on the cross-section of the welding joint for all CPs investigated using the *Struers* DURAMIN-40AC3 equipment. The used microhardness scale was 0.3 HV, with an indentation time of 10 seconds.

The electrochemical tests were performed using three electrodes: working electrode (ET), reference electrode (RE) of Ag/AgCl KCI$_{sat}$, and counter electrode (CE) of platinum wire. The areas analyzed in the welded joints CPs cross-section were the base metal (BM), fusion line (LF), welding root end welding face, Figure 2.

The degree of Cr depletion caused by microstructural modification during welding process was evaluated by Double Loop Electrochemical Potenciokinetic Reactivation test (DL-EPR), using a Solartron 1287 potentiostat. DL-EPR test was carried out in a minicell with a capillary of 1.5 mm diameter. The electrolyte was 0.5 mol.L^{-1} H$_2$SO$_4$ + 0.01 mol.L^{-1} KSCN. The test was performed after 05 minutes of open circuit potential (OCP). The electrochemical test was scanned in the anodic direction, from of -500 mV (Ag/AgCl) up to 300 mV (Ag/AgCl), and then reversed to -500 mV (Ag/AgCl),

with a scan rate of 1.67 mV/s. Pitting corrosion behavior was characterized by anodic polarization scans in an electrolyte of 3.5 wt.% NaCl with Syringe Cell method[25,26], with exposed area of 0.07 cm^2, using a Gamry PCI4/300 potentiostat. The tests were performed after stabilization on the OCP (5 min). The initial potential was -0.2 mV$_{OCP}$ and final potential,1.0 V$_{Ref}$ with scan rate of 1.67 mV/s. All tests were performed at least five times to confirm the reproducibility of the tests.

3. Results and Discussion

Macrographs of all samples cross-section - etched in 10 wt% oxalic acid solution - are shown in Figure 3a-f. With the metallographic attack it was possible to observe the shape and extent of the FZ in each CP. In the manual welding process, the FZ was irregular along its length, therefore, it was identified that the FZ was different for each CP. In relation to the weld root, it was observed that the CPs had an average extension of approximately 08 mm, and only CP 04 had an extension of 10 mm. For CP 04, a lower welding speed and higher heat input value were used. It was observed that between the CPs of two passes (CP 01, CP 02 and CP 03), for CP 01 and CP 03 the greater width of the FZ in the upper part of the cross-section of the weld, this was not observed for CP 02. As for the CPs with just one pass (CP 04, CP 05 and CP 06), only CP 06 presented a shorter FZ extension. For this CP, a lower heat input value and higher welding speed were used.

Figure 4a-h presented micrographs after etching in 10 wt% oxalic acid solution for all CPs studied and MB 2101.
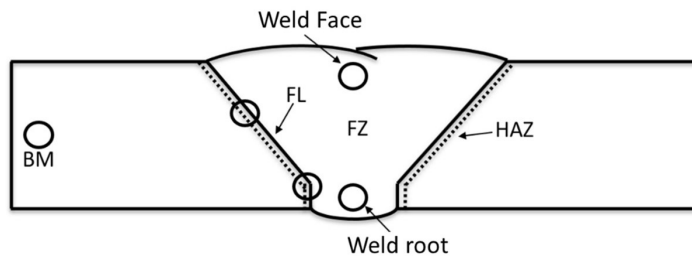

Figure 2. Diagram of the welded cross-section indicating mini capillary coupling points of corrosion tests (FZ: fusion zone; HAZ: heat affected zone; FL: fusion line; BM: base metal).
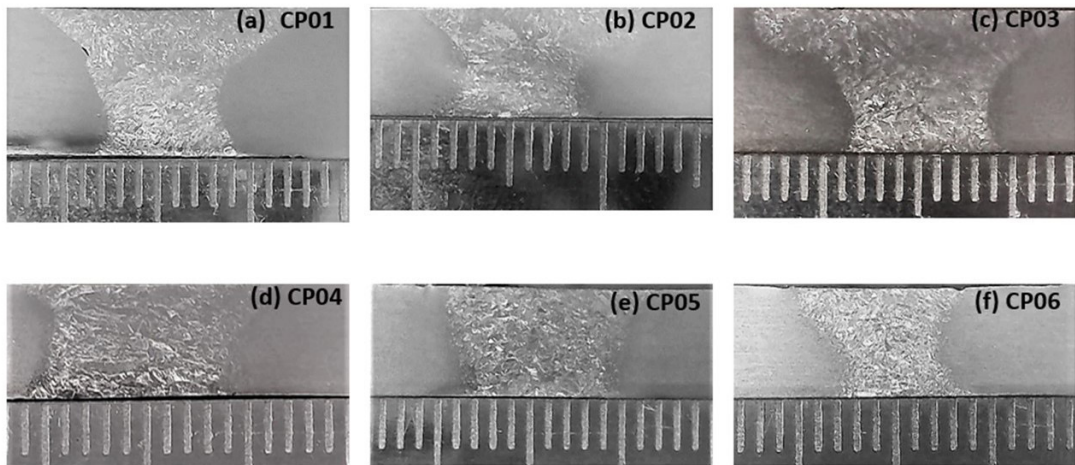

Figure 3. Macrographs of (a) CP 01, (b) CP 02, (c) CP 03, (d) CP 04, (e) CP 05 and (f) CP 06 after etching in 10 wt% oxalic acid solution.
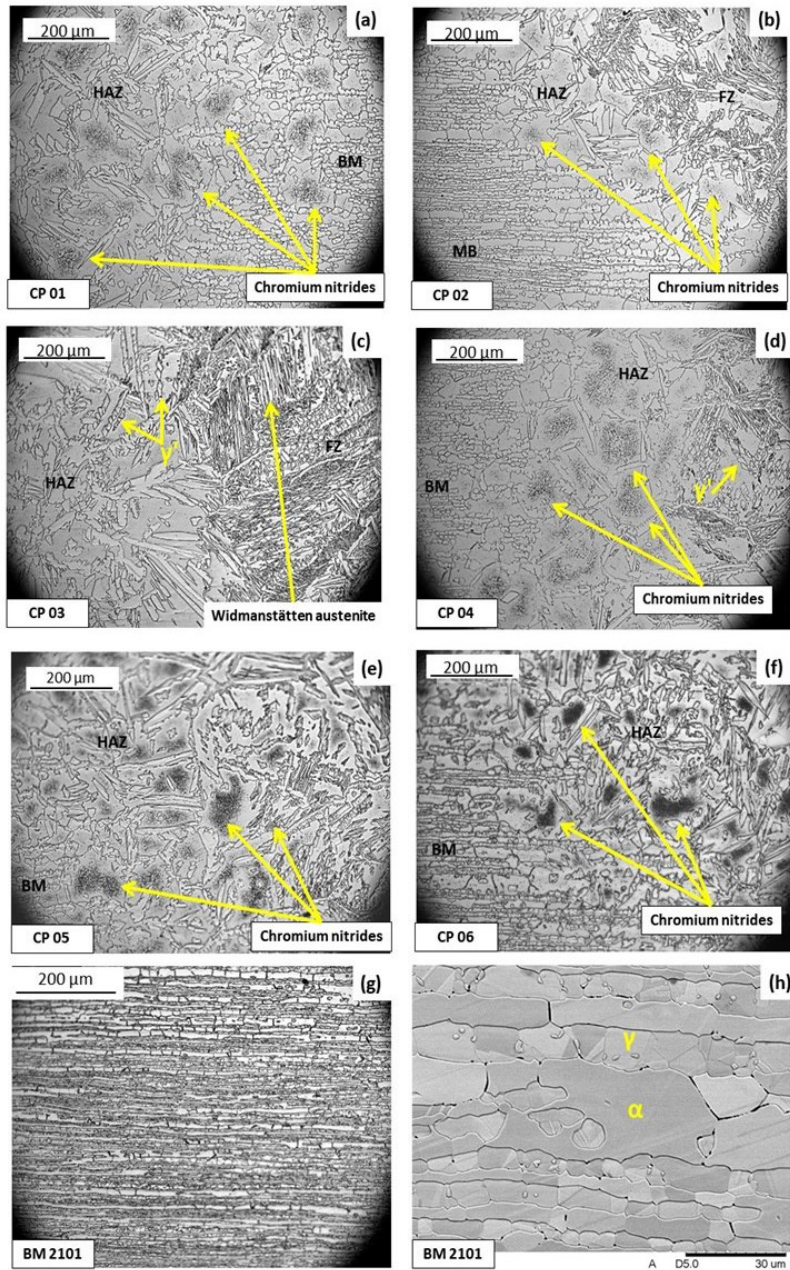
Figure 4. Micrographs of CPs (a) CP 01, (b) CP 02, (c) CP 03, (d) CP 04, (e) CP 05, (f) CP 06, (g) and (h) BM 2101. Etching in 10 wt% oxalic acid solution, at room temperature.

This attack revealed microstructural heterogeneities, such as interphase and grain boundaries, and particular areas with higher chromium contents[15,27,28].There are differences in the microstructure when analyzing the different regions (BM, HAZ and FZ). The BM presented elongated grains; characteristic of materials submitted to the lamination process, with ferrite (α) and austenite (γ). FZ presents a more elongated phase, in the form of laths. The literature[10,11,29] relates FZ to austenite grains in Widmanstätten laths, secondary austenite (γ2) and matrix of ferrite, as observed in Figure 3. More intense attacks were observed near FL, between FZ and HAZ regions. In the HAZ, complexes and combined microstructures were

also observed, with elongated grains like FZ, and smaller grains, similar to BM. In Table 1 it is observed that there is a difference in composition between BM UNS S32101 and ER2209, with Ni being the element with the greatest difference. Increasing the nitrogen content accelerates the reforming of austenite of different morphologies during cooling, in particular Widmanstätten austenite, and limits the thermal welding effect[30]. Corrosive attack was observed near FL. This type of attack is characterized by chromium nitride precipitates[1]. These precipitates were observed in higher number on the surface of CP 01 (two-pass conditions), CP 04 and CP 05 (one-pass conditions).

Study of Corrosion Resistance of Lean Duplex Stainless Steel 2101 Welded by the Gas Tungsten Arc Welding
Double Fusion (GTAW-DF) Process for Use in the Citrus Juice Industry

5

Figure 5a-f shows Vickers Microhardness maps along the cross-section of all CPs in all investigated conditions with different zones identification, such as BM, HAZ and FZ. The average microhardness of BM was approximately 248 HV. The ZF was the region with the highest microhardness values, between 255 HV and 284 HV, as indicated by the red and yellow colors in the maps. The difference in the values of the microhardness maps were not that significant. However, these results show that the welding process altered the microstructure and hardness of the material, especially in the HAZ region. The highest values of FZ are due to the welding filler metal ER2209, whose composition contains 8.6% of Ni, while MB has only 1.15%. The high Ni content stabilizes the austenite, resulting in hardness increasing. The other element that contributed to increase in hardness in the FZ was Mo, with 3.8%. this element is a strong solid solution strengthener, which contribute for increasing hardness in the region[8,30,31].

The effect of welding on the microstructure can be clearly identified in the HAZ regions, observed by microhardness variations, indicated in blue color. This variation was observed to all welding conditions and can be associated to solution annealing process of BM. The microhardness heterogeneity between BM and ZF confirms the importance of the welding process in the corrosion resistance properties. It is important to mention the possibility of galvanic coupling between the HAZ and the welding filler metal, which can result in preferential attack in the interface regions. It is also noted that the highest microhardness values were identified (red color) at the top of ZF in CP 01 (Figure 5a), particularly in the CPs welded with two passes, suggesting formation of hardening precipitates with the heat input. To on-pass CPs the indication of higher hardness was identified along the ZF. CP 04 and CP 05 with lower values of hardness along the HAZ. For these two conditions higher heat input values and lower welding speeds were used during the welding
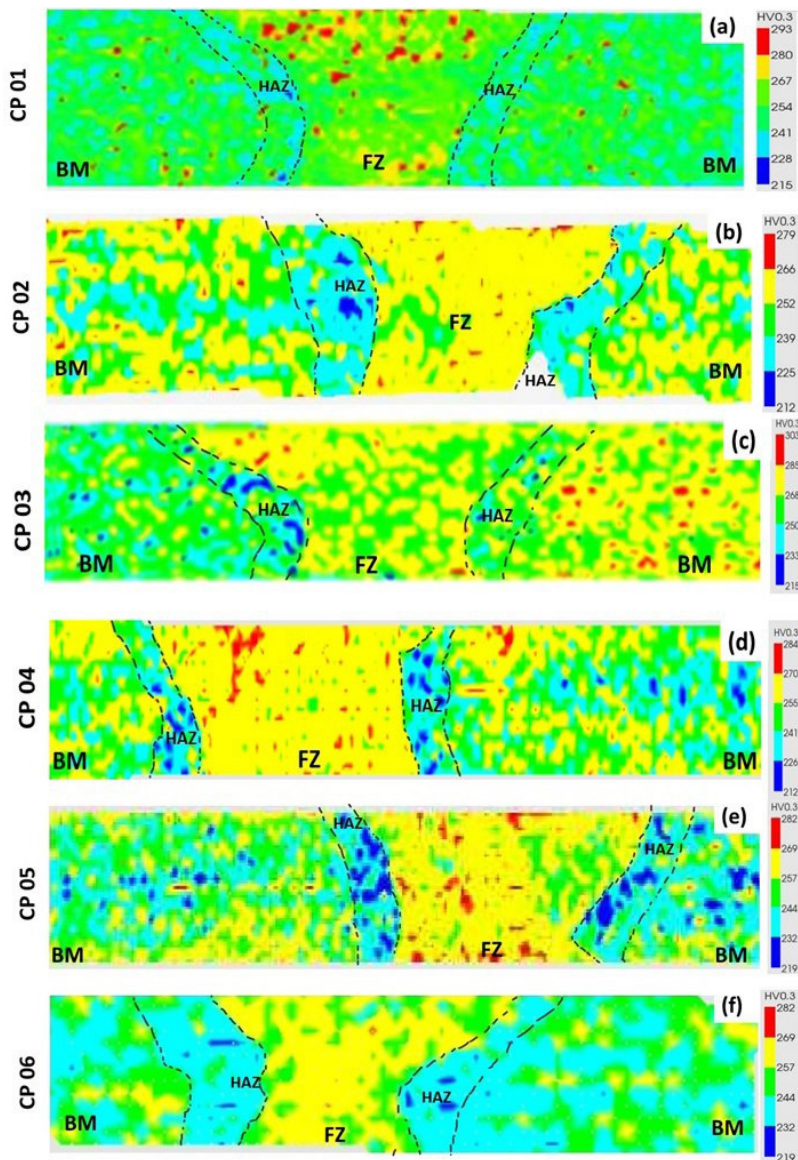

Figure 5. Vickers microhardness maps along the cross-section of all CPs investigated conditions.

process. Figure 6 presented DL-EPR curve to BM obtained in 0.5 mol.L^{-1} H$_2$SO$_4$ + 0.01 mol.L^{-1} KSCN solution. It is observed that the activation peak (i$_a$) occurs at 4.0 x 10-2 A/cm^2 and the reactivation peak (i$_r$), at 1.0 x 10-4 A/cm^2. The ratio (i$_r$/i$_a$) x 100% indicates the degree of sensitization of the material. For the base metal, this ratio was 0.25%.

Figure 7a, b shows DL-EPR curve to all CPs in the LF (weld root and weld top). The behavior of both zones and the BM was similar among the six welded conditions. In the BM curve (Figure 6) the line in red (i$_a$) is the maximum current that leads to the formation of the passive layer on the surface of the material, indicating the tendency to passivation. The blue line (i$_r$), on the other hand, shows the maximum reactivation current during the reverse scan, and indicates the tendency to localized attack. In the curve obtained in the reverse direction three corrosion potentials are observed, being the first one, at higher potentials, associated with the formation of the passive film, resulting in ennoblement of the corrosion potential. The second corrosion potential is because the cathodic and anodic currents in the reverse

direction are equalized during the reverse scan. The third potential is associated with the peak current density, or reactivation current.

Figure 8a, b shows the comparison of the in the ir/ia ratio of the all CPs in the LF, (welding root and welding top) obtained from the DL-EPR curves, in 0.5 mol.L^{-1} H$_2$SO$_4$ + 0.01 mol.L^{-1} KSCN electrolyte. Differences in cell positioning result in differences in the proportion of LF exposed areas of both UNS S32101 and ER2209, and variations in the results of the DL-EPR test, mainly observed in CP 01 and CP 02 in the LF root. For all conditions studied, it was observed that the welding process affected the intergranular corrosion resistance of the LF region, both root and top. The i$_r$/i$_a$ rate values found were higher than those presented by the BM. Reactivation peaks of the DL-EPR test can be attributed to the preferential corrosion attack of Cr-depleted regions around Cr-carbides or Cr-nitrides[1]. The Sensitization process occurs when stainless steel is subjected to high temperatures such as heat treatment processes, high operating temperatures or welding processes. These situations give rise to the precipitation of phases and precipitates other than ferrite and austenite, such as carbides and nitrides that are rich in Cr. Therefore, the reduction of this element in the vicinity of the contours makes the material more susceptible to intergranular corrosion[32]. It was observed how the change in microstructure and the effect of galvanic coupling influenced the resistance to intergranular corrosion of the material. In position 02, the CPs underwent two-passes (CP 01, CP 02 and CP 03), CP 02 was the one that showed the highest degree of sensitization in the lower FL. In position 07, welding top of the LF, CP 03 was the one with the lowest resistance to intergranular corrosion. In relation to one-pass CPs, the most susceptible to this type of corrosion was CP 04, followed by CP 05 and finally CP 06.

Figure 9 presents three polarization curves for MB UNS S32101 obtained after 5 minutes of OCP in a 3.5%wt. NaCl solution. The MB shows average values of Ecorr = -243 mV, Epite = 383 mV and ΔE = 627 mV. At potentials below the Epite, current oscillations typical of metastable pits are noticed. Figure 10 presents the average E$_{corr}$ values obtained from the polarization curves for the welding
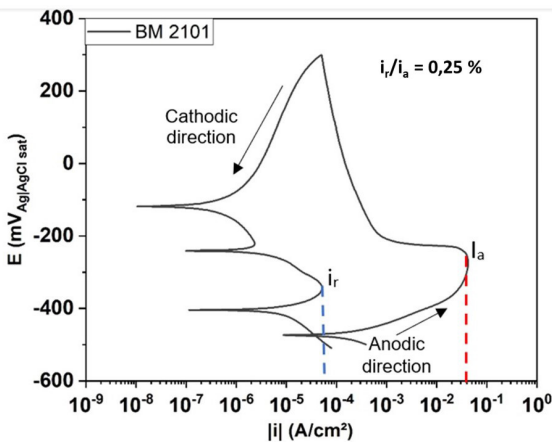

Figure 6. DL-EPR curves for the BM UNS S32101 0.5 mol·L^{-1} H$_2$SO$_4$ + 0.01 mol·L^{-1} KSCN solution, indicating the current density of activation (i$_a$) and reactivation (i$_r$).
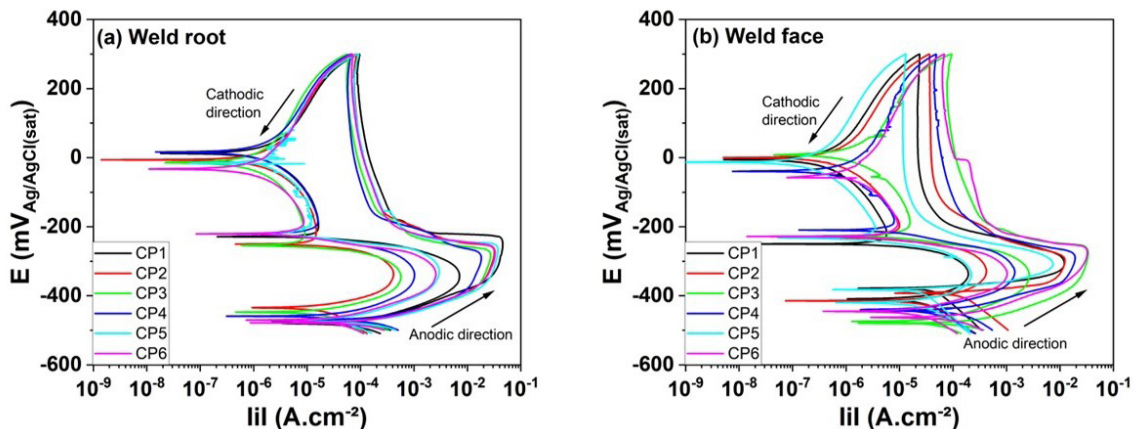

Figure 7. DL-EPR curves for the LF (a) weld root and (b) weld top positions in the different CPs, in 0.5 mol·L^{-1} H$_2$SO$_4$ + 0.01 mol·L^{-1} KSCN solution.

Study of Corrosion Resistance of Lean Duplex Stainless Steel 2101 Welded by the Gas Tungsten Arc Welding
Double Fusion (GTAW-DF) Process for Use in the Citrus Juice Industry

7

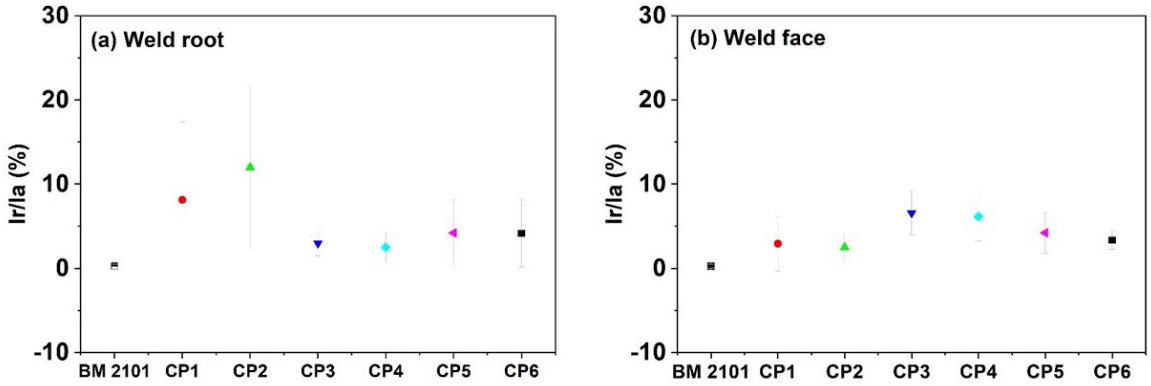**Figure 8.** Comparison of the i_r/i_a ratio CPs in the LF, (a) weld root and (b) weld top, obtained from the DL-EPR curves, in 0.5 mol·L^{-1} H$_2$SO$_4$ + 0. 01 mol·L^{-1} KSCN solution.
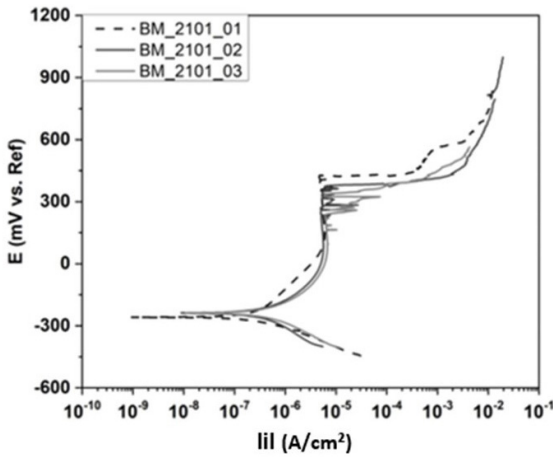

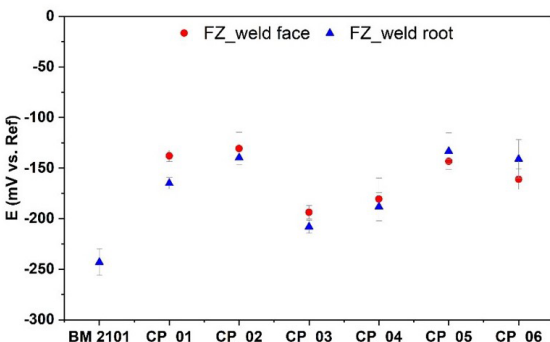**Figure 9.** Potentiodynamic polarization curves of BM UNS S32101 obtained in 3.5 wt% NaCl solution.

Figure 10. E$_{corr}$ values obtained from the potentiodymamic polarization curves for the FZ for all CPs studied in 3.5 w t.% NaCl solution.

Figure 11. E$_{corr}$, E$_{pit}$ and ΔE values obtained from the polarization curves for the (a) face and (b) root of the LF position of all CPs studied, 3.5 wt.% NaCl solution.

face and welding root after 5 minutes of OCP in 3.5 wt.% NaCl solution in the FZ. In this region it was not detected the breakdown potential. This is due to the ER2209 high concentration of Cr, Ni and Mo, favoring better corrosion resistance. The difference between the welding face and welding root of the FZ was also investigated in all samples and there were no significant differences in Ecorr values between the root and top part of the FZ. CP 03 and CP
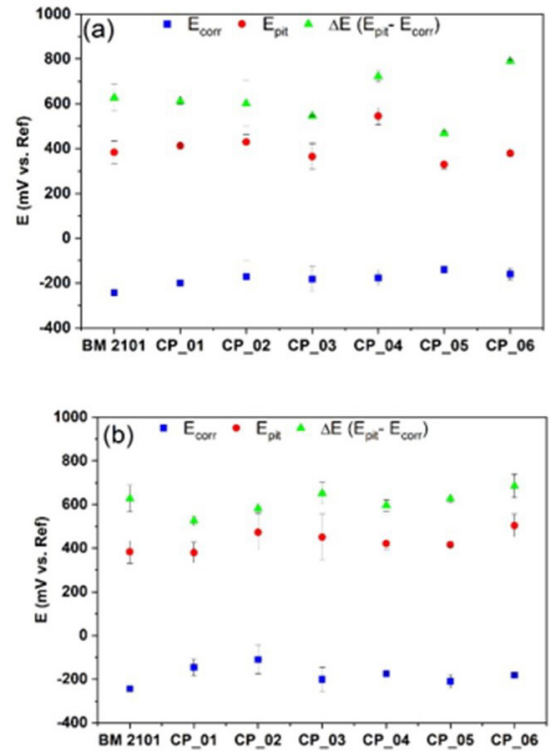
04 presented the lowest Ecor values. These two welding conditions presented the highest heat input for the two-pass and one-pass condition, respectively. These results suggest that the welding parameters used for CPs interfered in the corrosion resistance of ER2209 filler metal when compared to the other investigated conditions.

Figure 11a, b presents the average of ΔE (E$_{pit}$-E$_{corr}$) values for two positions of the LF of all studied conditions, the root and top LF. For all welding conditions, Ecorr values were close to –200 mV. However, when studying E$_{pite}$, a variation was observed between the CPs, the ΔE values were different for each CP. Higher ΔE values indicate

greater resistance to pitting corrosion. To compare the FL regions, where there is the effect of coupling between the HAZ of the BM LDX 2101 and the ER2209. In welding conditions with two-passes (CP 01, CP 02 and CP 03), a slight tendency towards an increase in ΔE from CP 01 to CP 03 was observed in the case of the region (root), however, the measurement variability was also greater for the CP 03. This suggests that the welding parameters in the two-pass condition affected the resistance to pitting corrosion in the FL region, which is the region that includes the HAZ and FZ. In these CPs, the weld root region is influenced by the first and second passes. The one-pass CPs, the results indicate an increase in the value of ΔE of CP 04 < CP 05 < CP 06, suggesting that the welding parameters in one-pass also affect the resistance to localized corrosion of duplex steel 2101. However, they follow a trend, that is, it was observed that the greater the heat input and the lower the detachment speed, the lower the resistance to pitting corrosion in the LF region of the samples welded with just one-pass.

4. Conclusion

In this work, six different GTAW-DF welding conditions for LSSD UNS S32101 welding were investigated. The different values of heat input were selected based on the adequate evolution in the execution of the welding aiming at the reduction of discontinuities and high productivity in the manufacturing process.

The effect of the welding parameters was observed on the microstructural change and on the corrosion resistance near LF of the CPs. DL-EPR tests identified susceptibility to intergranular corrosion in all CPs studied. Polarization tests with the Syringe Cell method proved to be effective, with absence of crevices and good reproducibility.

For the conditions of two-pass, it was observed that the CP with the highest heat inputs, not only in the first but also in the second pass, was the one that presented higher corrosion resistance. For the conditions welded with one-pass, it was observed that the CP with lower heat input and higher travel speed was the one that presented better results of corrosion resistance. It was also noticed the effect of galvanic coupling between the base metal (LDSS UNS S32101) acting as anode and filler metal (ER2209) as cathode.

5. Acknowledgments

6. References

1. Guilherme LH, Reccagni P, Benedetti AV, Fugivara CS, Engelberg DL. Corrosion assessment of ASME qualified welding procedures for grade 2101 lean duplex stainless steel. Corrosion. 2019;75(10):1216-29.

2. Lippold JC, Kotecki DJ. Welding metallurgy and weldability of stainless steels. New Jersey: John Wiley & Sons; 2005.

3. Gunn RN. Duplex stainless steels. Cambridge: Woodhead; 1997.

4. Senatore M, Finzetto L, Perea E. Estudo comparativo entre os aços inoxidáveis dúplex e os inoxidáveis AISI 304L/316L. REM Rev Escola Minas. 2007;60(1):175-81.

5. Kahar SD. Duplex stainless steels-an overview. Int J Eng Res Appl. 2017;7(4):27-36.

6. da Costa e Silva, ALV, Mei, PR. Aços e Ligas Especiais, 2nd ed. São Paulo: Editora Edgard Blücher; 2006, p. 407-431.

7. Padilha AF. Aços inoxidáveis austeníticos. Curitiba: Hemus; 1994.

8. Westin EM, Brolund B, Hertzman S. Weldability aspects of a newly developed duplex stainless steel LDX 2101. Steel Res Int. 2008;79(6):473-81. http://doi.org/10.1002/srin.200806155.

9. Makhdoom MA, Ahmad A, Kamran M, Abid K, Haider W. Microstructural and electrochemical behavior of 2205 duplex stainless steel weldments. Surf Interfaces. 2017;9:189-95. http://doi.org/10.1016/j.surfin.2017.09.007.

10. Westin EM, Hertzman S. Element distribution in lean duplex stainless steel welds. Weld World. 2014;58(2):143-60.

11. Sicupira DC, Frankel GS, Lins VFC. Pitting corrosion of welds in UNS S32304 lean duplex stainless steel. Mater Corros. 2016;67:440-8.

12. Yang Y, Yan B, Li J, Wang J. The effect of large heat input on the microstructure and corrosion behaviour of simulated heat affected zone in 2205 duplex stainless steel. Corros Sci. 2011;53(11):3756-63.

13. Zhang Z, Jing H, Xu L, Han Y, Zhao L. Investigation on microstructure evolution and properties of duplex stainless steel joint multi-pass welded by using different methods. Mater Des. 2016;109:670-85.

14. Aguiar IV, Escobar DP, Santos DB, Modenesi PJ. Microstructure characterization of a duplex stainless steel weld by electron backscattering diffraction and orientation imaging microscopy techniques. Materia (Rio J). 2015;20(1):212-26.

15. Silva R, Baroni LFS, Kugelmeier CL, Silva MBR, Kuri SE, Rovere CAD. Thermal aging at 475 °C of newly developed lean duplex stainless steel 2404: mechanical properties and corrosion behavior. Corros Sci. 2017;116:66-73.

16. Westin EM. Microstructure and properties of welds in the lean duplex stainless steel LDX 2101 [thesis]. Stockholm: Royal Institute of Technology; 2010.

17. Valeriano LC, Correa EO, Mariano NA, Robin ALM, Machado MAGTC. Influence of the solution-treatment temperature and short aging times on the electrochemical corrosion behaviour of Uns S32520 super duplex stainless steel. Mater Res. 2019;22(4):22.

18. Antunes PD, Silva CC, Corrêa EO. Effect of the heat input and ageing treatment on microstructure and mechanical properties of AISI 317L stainless steel dissimilar welded joints. Mater Res. 2022;25:e20220118.

19. Conceição JN, Correa EO, Gonzaga AC, Pardal JM, Tavares SSM. Mechanical properties of UNS S39274 superduplex stainless steel work hardened and solution annealed. Mater Res. 2022;25:e20220108.

20. Antunes PD, Silva CC, Correa EO, Tavares SSM. Influence of the heat input and aging treatment on microstructure and mechanical properties of AISI 317 L steel weldments using 0020 robotic–pulsed GMAW. Int J Adv Manuf Technol. 2019;105(12):5151-63.

21. Mohammed GR, Ishak M, Aqida SN, Abdulhadi HA. Effects of heat input on microstructure, corrosion and mechanical characteristics of welded austenitic and duplex stainless steels: a review. Metals. 2017;7(2):39.

22. Mohammed Asif M, Shrikrishna KA, Sathiya P, Goel S. The impact of heat input on the strength, toughness, microhardness, microstructure and corrosion aspects of friction welded duplex stainless steel joints. J Manuf Process. 2015;18:92-106.

23. Zhang YM, Zhang SB. Double-sided arc welding increases weld joint penetration. Welding Journal (Miami, Fla). 1998;77:57-61.

24. Qiang W, Wang K. Shielding gas effects on double-sided synchronous autogenous GTA weldability of high nitrogen austenitic stainless steel. J Mater Process Technol. 2017;250:169-81.

25. Hernández JWC, de Souza Carvalho Machado C, Costa I, de Melo HG. Technical note: syringe cell to avoid crevice corrosion on stainless steels during potentiodynamic polarization testing. Corrosion. 2021;77(12):1274-7.

Study of Corrosion Resistance of Lean Duplex Stainless Steel 2101 Welded by the Gas Tungsten Arc Welding
Double Fusion (GTAW-DF) Process for Use in the Citrus Juice Industry

9

26. Panindre AM, Chang KH, Weirich T, Frankel GS. Technical note: syringe cell for electrochemical testing. Corrosion. 2018;74(8):847-50.

27. Deng B, Jiang Y, Xu J, Sun T, Gao J, Zhang L, et al. Application of the modified electrochemical potentiodynamic reactivation method to detect susceptibility to intergranular corrosion of a newly developed lean duplex stainless steel LDX2101. Corros Sci. 2010;52(3):969-77. http://doi.org/10.1016/j.corsci.2009.11.020.

28. Gao J, Jiang Y, Deng B, Zhang W, Zhong C, Li J. Investigation of selective corrosion resistance of aged lean duplex stainless steel 2101 by non-destructive electrochemical techniques. Electrochim Acta. 2009;54(24):5830-5.

29. Sicupira DC, Cardoso R Jr, Bracarense AQ, Frankel GS, Lins VFC. Cyclic polarization study of thick welded joints of lean duplex stainless steel for application in biodiesel industry. Mater Res. 2017;20(1):161-7.

30. Kellai A, Lounis A, Kahla S, Idir B. Effect of root pass filler metal on microstructure and mechanical properties in the multi-pass welding of duplex stainless steels. Int J Adv Manuf Technol. 2018;95(9-12):3215-25.

31. Zhang Z, Jing H, Xu L, Han Y, Zhao L, Zhang J. Influence of microstructure and elemental partitioning on pitting corrosion resistance of duplex stainless steel welding joints. Appl Surf Sci. 2017;394:297-314.

32. Tavares SSM, Silva MR, Pardal JM, Silva MB, de Macedo MCS. Influence of heat treatments on the sensitization of a supermartensitic stainless steel. Cienc Tecnol Mater. 2017;29(1):e1-8.